IEEE Access
Multidisciplinary | Rapid Review | Open Access Journal

Received November 15, 2019, accepted November 28, 2019, date of publication December 2, 2019,
date of current version December 23, 2019.

Digital Object Identifier 10.1109/ACCESS.2019.2957243

Mobile Energy Storage Sizing and Allocation for Multi-Services in Power Distribution Systems

HUSSEIN ABDELTAWAB[1], (Member, IEEE), AND YASSER ABDEL-RADY I. MOHAMED[2], (Senior Member, IEEE)

[1]Division of Business, Engineering, and Information Sciences and Technology, Penn State Altoona, Altoona, PA 16601, USA
[2]Department of Electrical and Computer Engineering, University of Alberta, Edmonton, AB T6G 2V4, Canada

Corresponding author: Hussein Abdeltawab (hza5222@psu.edu)

This work was supported in part by Alberta Innovates, and in part by the Future Energy Systems Research through the Canada First Research Excellence Fund (CFREF).

ABSTRACT A mobile energy storage system (MESS) is a localizable transportable storage system that provides various utility services. These services include load leveling, load shifting, losses minimization, and energy arbitrage. A MESS is also controlled for voltage regulation in weak grids. The MESS mobility enables a single storage unit to achieve the tasks of multiple stationary units at different locations. The MESS is connected to the grid at specific substations (or buses) known as MESS stations. This paper proposes an optimization algorithm for sizing and allocation of a MESS for multi-services in a power distribution system. The design accounts for load variation, renewable resources intermittency, and market price fluctuations. A realistic dynamic model for the MESS is adopted to consider the capacity and lifetime constraints. A detailed network power flow model is utilized to include voltage constraints, feeders, and transformers ampacity in the problem formulation. By considering all these constraints, the resulting sizing problem is a mixed-integer nonlinear problem. This paper presents the problem formulation and proposes a solution using a hybrid optimization technique. The adopted technique is based on the particle swarm algorithm and mixed-integer convex programming. A case study is conducted on a real 41-bus radial feeder to validate the proposed sizing technique, and investigate the MESS profitability to the system operator.

INDEX TERMS Energy storage sizing, distributed storage allocation, power converter cost, mobile energy storage.

NOMENCLATURE

Acronyms:

DG	Distributed Generation
Disco	Distribution Company
MESS	Mobile Energy Storage System
SESS	Stationary Energy Storage System
PSO	Particle Swarm Optimization
RES	Renewable Energy Source

Sets, Indices:

$\mathcal{N}^{MES}$	Set of buses MESS is allowed to be allocated at.
$\mathcal{N}^{bus}$	Set of all system buses.
$\mathcal{N}^{tr}$	Set of time instants that MESS is in transit.
j	Index for PSO iterations.
m	Index for swarm population size.
i	Current MESS Bus index at time t.
l	Branch (line or transformer) index.
sc	Index of a certain generation scenario.
t	Hourly index in a certain year and scenario.
y	Planning year index in a certain scenario.

Parameters:

$\frac{dp^{loss}}{dP^{bus}}\Big\|_{sc,y,t}$	Loss sensitivity to active power change at hour t, year y, scenario sc.
$\frac{dq^{loss}}{dP^{bus}}\Big\|_{sc,y,t}$	Loss sensitivity to reactive power change at hour t, year y, scenario sc.
$\frac{dv^{loss}}{dP^{bus}}\Big\|_{sc,y,t}$	Voltage sensitivity to active power change at hour t, year y, scenario sc.
$\frac{dv^{loss}}{dQ^{bus}}\Big\|_{sc,y,t}$	voltage sensitivity to reactive power change at hour t, year y, scenario sc.
$\overline{TN^{MES}}$	Total MESS number of cycles.
$\overline{z}^{MES}$	Maximum number of MESS stations.
$\overline{\mathbb{E}^{MES}}$	Maximum allowable MESS energy rating.

The associate editor coordinating the review of this manuscript and approving it for publication was Amjad Anvari-Moghaddam.

$\overline{\mathbb{S}^{MES}}$	Maximum allowable MESS power rating.
$C^{MES/MVA}(\mathbb{S}^{MES})$	MESS per-unit power cost for each MVA installed as a function in the rated capacity.
$C^{MES/MWh}$	MESS per-unit Energy cost for each MWh installed.
C^{truck}	MESS truck initial cost.
C^{Tr}	MESS cost of delay in transit.
$\overline{DT}$	Maximum number of daily trips made by MESS.
d_i	Delay Time in hours in case the storage truck moved from bus i at time t-1 to future bus at time t.
$\overline{J}$	Maximum number of iteration for PSO algorithm.
$O\&M_y^{MES}$	MESS operation and maintenance cost at year y.
$ip^{loss}_{sc,y,t}$	Initial system power losses at hour t, year y, scenario sc.
$iv^{loss}_{sc,y,t}$	Initial system nodal voltage at hour t, year y, scenario sc.
$\underline{v}$, $\overline{v}$	Minimum and maximum voltage limits in PU.
$\mathbb{S}^f(l)$	Feeder l current carrying capacity in MVA.
α^{TN}	MESS energy size extension factor.
η^{ch}	MESS charging efficiency.
η^{dc}	MESS discharging efficiency.
$\lambda^{load}_{sc,y,t}$	Reactive to active load power ratio at hour t, year y, scenario sc.
ρ_{sc}	The probability of scenario sc.
ω_{max}	Maximum inertia for PSO algorithm.
ω_{min}	Minimum inertia for PSO algorithm.
Y	Project life in years.
$FC^{MES}(i)$	Fixed cost of MES station's installation at bus i.
IR	Interest rate.
$bp_{sc,y,t}$	Energy buying price at hour t, year y, scenario sc.
inc	Disco income during the planning period
$sp_{sc,y,t}$	Energy selling price at hour t, year y, scenario sc.
γ	Number of iterations which PSO stops after, in case the profit difference stills down with certain tolerance.
ε	Cost function change tolerance at which the PSO escapes iterations and stops.
τ	Optimization sample time in hours.
$p^{load}_{sc,y,t}(i)$	load active power at bus i at hour t, year y, scenario sc.

Decision Variables:

$p^{res}_{sc,y,t}(i)$	RES active power at bus i at hour t, year y, scenario sc.
$\Delta p^{bus}_{sc,y,t}(i)$	Active power change of bus i at hour t, year y, scenario sc.
$\Delta q^{bus}_{sc,y,t}(i)$	Reactive power change of bus i at hour t, year y, scenario sc.
$E^{MES}_{sc,y,t}$	MESS energy at hour t, year y, scenario sc.
$N^{MES}_{sc,y,t}$	MESS current number of cycles at hour t, year y, scenario sc.
$ch^{MES}_{sc,y,t}(i)$	MESS charging power at bus i at hour t, year y, scenario sc.
c^{MES}	Total MESS operation and capital cost.
c^{grid}	Total cost of energy purchasing from the grid.
$dc^{MES}_{sc,y,t}(i)$	MESS discharging power at hour t, year y, scenario sc.
$p^{grid}_{sc,y,t}$	Grid active power at hour t, year y, scenario sc.
$p^{MES}_{sc,y,t}(i)$	MESS active power at bus i at hour t, year y, scenario sc.
$p^{bus}_{sc,y,t}(i)$	Total bus i active power at hour t, year y, scenario sc.
$p^{f}_{sc,y,t}(l)$	Feeder l active power flow at hour t, year y, scenario sc.
$p^{loss}_{sc,y,t}$	System final active power losses at hour t, year y, scenario sc.
$q^{grid}_{sc,y,t}$	Grid reactive power at hour t, year y, scenario sc.
$q^{MES}_{sc,y,t}(i)$	MESS reactive power at bus i at hour t, year y, scenario sc.
$q^{bus}_{sc,y,t}(i)$	Total bus i reactive power at hour t, year y, scenario sc.
$q^{f}_{sc,y,t}(l)$	Feeder l reactive power flow at hour t, year y, scenario sc.
$q^{loss}_{sc,y,t}$	System final reactive power losses at hour t, year y, scenario sc.
$s^{f}_{sc,y,t}(l)$	Feeder l apparent power flow at hour t, year y, scenario sc.
$x^{MES}_{sc,y,t}(i)$	Binary existence index for the MESS at the station located at bus i at hour t, year y, scenario sc.
$y_m(j)$	Particle m value at iteration j.
$z^{MES}(i)$	Binary indicator for MESS station existence at bus i.
$\mathbb{E}^{MES}$	MESS rated Capacity in MWh.
$\mathbb{S}^{MES}$	MESS rated power in MVA.
$DT_{sc,y,t=24}$	[2pt] Daily number of the trips made at the end of a certain day at year y in scenario sc.
pro	Disco profit during the planning period.
$\mathcal{R}pro$	Disco real profit after considering MESS delay effect.
$\mathbb{Y}(j)$	PSO total population at iteration j.
$\omega(j)$	PSO inertia value at iteration j.

I. INTRODUCTION

The distribution power system structure is evolving to fit the increasing renewable energy sources penetration. Recent research shows that for every 10% wind penetration, a 2-4% balancing generation is needed for stable operation [1]. The renewable energy future goes hand in hand with energy storage systems (ESSs). An ESS can provide various grid support services due to its fast time-response and various power and energy density in different technologies. As a result, ESSs have various applications for both the energy and transport sectors as explained in [2]. The economic benefit of ESSs is feasible when combined with renewable resources, such as PV or wind farms for power regulation [3], [4]. Optimal sizing of ESS for these applications is key for a successful investment [5], [6]. With the increasing number of RESs dispersed in the system, a large number of ESSs is needed to support grid stability and reliability. Because ESSs are relatively expensive for their lifetime, distributed ESSs represent an expensive RES integration solution.

The ESS per-unit cost decreases radically with its size; thus, a large number of distributed ESSs is more expensive than a single ESS (given the same capacity).

For instance, the ESS power conversion system per-unit cost varies from (1,800$/kW) for a 5 kW station to (300$/kW) for a 2 MW one [7]. Thus, a significant saving is achievable if a single bulk ESS can replace a large number of smaller ESSs. On the other side, distributed ESSs provide essential services that a single centralized ESS cannot provide, such as voltage regulation and power losses minimization. A MESS can provide a solution for the aforementioned trade-off. A MESS is a single ESS plugged into the system at different locations during different times [8]. It can be regarded as a distributed ESSs working at different times but a cheaper alternative. The main advantage of the MESS is the transportability that enables delivering a localized reactive/active power support for voltage regulation, power loss reduction, and dispersed RESs integration.

Stationary ESSs planning has been widely discussed in the literature on several levels: distribution system level [9]–[11], renewable energy integration [12], [13]; AC transmission system level [14]–[16]; DC transmission system level [17]; and autonomous micro-grids [18]–[21]. The work in [22] investigates MESS sizing for improving power system reliability and better RES integration. Another study for reliability improvement using a MESS is proposed in [23]. Regarding the MESS energy management and control, the work in [8] proposes the day-ahead scheduling of the MESS. However, to the best of the authors' knowledge, the problem of sizing MESS for multi-tasking in the power distribution system needs further investigation. The main contribution of this work is the development of a MESS sizing/allocation framework that maximizes the Disco profit by participating in multi-tasks. Another contribution to the sizing problem is considering the variable cost nature of the power converter.

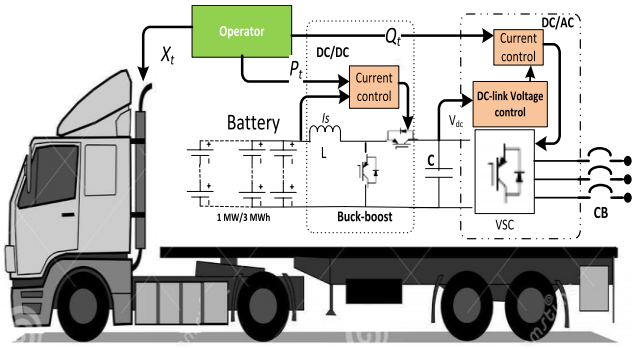

FIGURE 1. MESS structure.

On the power industry and research levels, the MESS has witnessed some interest lately. First, a MESS project has been conducted by the Electric Power Research Institute (EPRI) in the USA [24], [25]. A 40 kVA MESS project has been implemented to increase network reliability [26]. Another project proposes a 500 kW storage for the tea industry peak shaving in China [27]. MESSs are available commercially in 100 to 5000 kW sizes [28]. Another project designs a 500 kW/776 kWh MESS for peak shaving and voltage regulation in Spain [29]. This paper helps in solving the sizing problem for such projects.

The research in this paper is initially developed as part of the first author's Ph.D. research work [30]. The thesis presents planning and operation algorithms of energy storage in active distribution systems, whereas this paper focuses on the sizing and planning of MESS in more depth. This paper is arranged as follows. First, the problem is formulated in Section II. Section III presents the hybrid optimization sizing algorithm whereas Section IV presents a case study on a typical real radial feeder in Ontario-Canada. Finally, the conclusions are drawn in Section V.

II. PROBLEM FORMULATION

The MESS consists of an ESS carried on a truck as shown in Figure 1. The ESS is an array of battery cells (e.g., lithium-ion). The array is connected to the grid via a DC/DC/AC four-quadrant voltage-source converter (VSC) [31]. The MESS operator can directly control the active power (e.g., peak shaving mode) and reactive power (e.g., voltage regulation mode). The operator must define the truck desired bus location (station x_t) at any time. The MESS is controlled to maximize the distribution company (Disco) profit and maintaining an acceptable power quality level (e.g., the voltage drop less than 5%, and acceptable branches ampacity). These objectives are achieved by simultaneously participating in multi-services such as energy arbitrage, power losses minimization, and voltage regulation. The MESS sizing technique should consider the previous objectives under different loads, RESs, and market scenarios. This section discusses the sizing problem formulation,

whereas Section III solves the problem by the proposed hybrid optimization technique.

A. THE OBJECTIVE FUNCTION

To simplify the formulation, the following terminology is adopted. For any variable $x_t^y(i)$, x is the parameter/variable name (e.g., p: power,); y represents the associated technology description (e.g., ES, DG), t is a future time index (e.g., sc: scenario, y: year index, t: hour index); finally, i is the location index (e.g., i; bus index, l: branch index). For example $q^{ES}_{sc,y,t}(i)$ is the reactive power injected by an ESS located at bus i in the case of scenario sc at the time sample t of the planning year y. The cost function presents the Disco profit during the planning horizon as given in (1). The cost function pro is calculated at each sample t indexed in an operation year y in a certain operation scenario sc. Each operation scenario sc has a certain probability ρ_{sc} such that $\sum_{sc}\rho_{sc}=1$. A scenario represents a different load, PV, wind, load power, and market price combinations.

$$Max(pro = inc - c^{grid} - c^{MES} - c^{Tr}) \tag{1}$$

$$inc = \sum\nolimits_{sc}\rho_{sc}\sum\nolimits_{y}\sum\nolimits_{t} sp_{sc,y,t}\sum\nolimits_{i} p^{Load}_{sc,y,t}(i)\,\tau \tag{2}$$

$$c^{grid} = \sum\nolimits_{sc}\rho_{sc}\sum\nolimits_{y}\sum\nolimits_{t} bp_{sc,y,t}p^{grid}_{sc,y,t}\tau \tag{3}$$

$$\begin{aligned} c^{MES} = {} & C^{truck} + \sum\nolimits_{i} z^{MES}(i)\,FC^{MES}(i) \\ & + C^{MES/MVA}(\mathbb{S}^{ES})\mathbb{S}^{ES} + C^{MES/MWh}\left(1+\alpha^{TN}\right) \\ & \times \mathbb{E}^{MES} + \sum\nolimits_{y}\frac{O\&M^{MES}_{y}}{(1+IR)^{Y-1}} \end{aligned} \tag{4}$$

$$\begin{aligned} c^{Tr} = {} & \sum\nolimits_{sc}\rho_{sc}\sum\nolimits_{y}\sum\nolimits_{t} sp_{sc,y,t}\sum\nolimits_{i}\frac{d_i}{\tau}ch^{MES}_{sc,y,t}(i) \\ & - \sum\nolimits_{sc}\rho_{sc}\sum\nolimits_{y}\sum\nolimits_{t} bp_{sc,y,t}\sum\nolimits_{i}\frac{d_i}{\tau}dc^{MES}_{sc,y,t}(i) \end{aligned} \tag{5}$$

$$d_i = \sum_{i}\left|x^{MES}_{sc,y,t}(i) - x^{MES}_{sc,y,t-1}(i)\right| d_{x^{MES}_{sc,y,t-1}(i)\to x^{MES}_{sc,y,t}(i)} \tag{6}$$

The Disco profit results from the income inc resulting from selling energy to the consumers with a selling price higher than the buying price that the Disco pays to buy this energy. The load power $p^{Load}_{sc,y,t}$ is sold for a price $sp_{sc,y,t}$. This price depends on the Disco tariff. Each Disco buys the power $bp^{grid}_{sc,y,t}$ from the energy market for a variable wholesale buying price $bp_{sc,y,t}$ from the energy market. The buying price witnesses a big change from off-peak to peak-hours, depending on the market volatility. The Disco can manage the MESS to perform load shifting for reducing the purchased energy c^{grid} during peak-hours.

The MESS capital and running costs consist of

1) The truck capital cost (TC).

2) The MESS stations cost FC^{MES}. It is a fixed cost that represents the construction cost of each station.

3) The storage power converter cost $C^{MES/MVA}$. This cost varies with the converter size with a nonlinear function as shown in Figure 1. The data are adapted from the average power conversion source cost provided in the EPRI report [7].

4) The battery bank cost $C^{MES/MWh}$. Future battery extension cost is defined by setting the parameter α^{TN}; this may be the case to reach a certain number of cycles TN by the end of the project life [32].

5) The MESS operation and maintenance costs $O\&M^{MES}$ are calculated yearly and transferred to the first year, depending on the interest rate IR during the project life y [11]. If the inflation rate is significant, it can be included to calculate the effective interest rate as explained in [33]. The maintenance cost includes the expected truck and ESS periodical maintenance cost, whereas the operation cost includes the MESS driver stipend and the truck yearly commute cost (gasoline cost, oil change cost, etc.)

6) Transition delay cost. When the MESS moves from a station to another, the system operator (Disco) compensates for the MESS delay by trading with the grid as follows. The Disco sells excessive RESs power to the grid at the selling price, or it buys power from the grid in the case of a power shortage. This cost is represented in the cost c^{Tr} which represents the cost of the transition delay at all operation times. If the MESS stayed at the same station, the transition-delay from sample $t-1$ to t is zero and the transition cost is zero as given in (6). Otherwise, the transition delay is counted for as a cost as given in (5).

B. THE MESS MODEL

The MESS model is different from the stationary ESS due to its varying location in the distribution network, as given in (7). The constraint in (7) states that the location of the MESS $x^{MES}_{sc,y,t}(i)$ is unique at a single station of the MESS stations that belong to the buses set $\mathcal{N}^{MES}$. Another important factor is the number of daily trips DT conducted by the MESS which is expressed in (8). If the MESS stayed the whole day at the same station $i=a$, then $\sum_{t=1}^{24} x^{MES}_{sc,y,t} - x^{MES}_{sc,y,t-1} = 0\ \forall i$ which means that no trips are made. On the other hand, if the MESS moved from a station a to another one b at a time α, then $\left|x^{MES}_{sc,y,\alpha+1}(a) - x^{MES}_{sc,y,\alpha}(a)\right| = \left|x^{MES}_{sc,y,\alpha+1}(b) - x^{MES}_{sc,y,\alpha}(b)\right| = 1$ which means that DT is accumulated by one each time a transition is made. The daily number of trips is upper bounded in (9).

$$\sum_{i} x^{MES}_{sc,y,t}(i) = 1 \quad \forall i \in \mathcal{N}^{MES} \tag{7}$$

$$DT_{sc,y,t=24} = \frac{\sum_{t=1}^{24}\sum_{i}\left|x^{MES}_{sc,y,t}(i) - x^{MES}_{sc,y,t-1}(i)\right|}{2} \tag{8}$$

$$DT_{sc,y,t=24} \le \overline{DT} \tag{9}$$

The stations' location and sizing of a MESS are expressed in (10)-(12). The binary variable $z^{MES}(i)$ indicates that the bus i is chosen to host a MESS station. The number of stations is limited in (10), whereas the station maximum power $\overline{\mathbb{S}^{MES}}$ is upper bounding the MESS rated power $\mathbb{S}^{MES}$ in (11). The MESS maximum allowable capacity $\overline{\mathbb{E}^{MES}}$ is

expressed in (12).

$$\sum_i z^{MES}(i) \le \bar{z}^{MES} \quad \forall i \in \mathcal{N}^{MES} \tag{10}$$

$$0 \le \mathbb{S}^{MES} \le z^{MES}(i)\,\overline{\mathbb{S}^{MES}} \tag{11}$$

$$0 \le \mathbb{E}^{MES} \le z^{MES}(i)\,\overline{\mathbb{E}^{MES}} \tag{12}$$

The MESS power consists of two mutually exclusive terms, the charging power $ch^{MES}_{sc,y,t}$ (positive) and discharging power $dc^{MES}_{sc,y,t}$ (negative), as shown in (13). The constraint states that the MESS is only allowed to charge or discharge at a certain station i only if it is located at this station at this time. The rated power constraints are imposed in (14)-(15). The reactive power is limited by (16). The reactive power is injected/absorbed at any bus for power quality purposes. Finally, the converter thermal limit is defined in (17) for the kVA rating. It is worth mentioning that the constraints (14)-(17) are nonlinear because $\mathbb{S}^{MES}$ and $x^{MES}_{sc,y,t}(i)$ are decision variables.

$$p^{MES}_{sc,y,t}(i) = ch^{MES}_{sc,y,t}(i) + dc^{MES}_{sc,y,t}(i) \tag{13}$$

$$0 \le ch^{MES}_{sc,y,t}(i) \le \mathbb{S}^{MES} x^{MES}_{sc,y,t}(i) \tag{14}$$

$$-\mathbb{S}^{MES} x^{MES}_{sc,y,t}(i) \le dc^{MES}_{sc,y,t}(i) \le 0 \tag{15}$$

$$-\mathbb{S}^{MES} x^{MES}_{sc,y,t}(i) \le q^{MES}_{sc,y,t}(i) \le \mathbb{S}^{MES} x^{MES}_{sc,y,t}(i) \tag{16}$$

$$p^{MES}_{sc,y,t}(i)^2 + q^{MES}_{sc,y,t}(i)^2 \le x^{MES}_{sc,y,t}(i)\,\mathbb{S}^{MES^2} \tag{17}$$

Regarding the battery capacity sizing, the capacity at any time is modeled as an integrator of the power injected/absorbed at any station i. Both the charging and discharging efficiencies η^{ch}, η^{dc} are considered as in (18). The MESS capacity is upper-bounded by its rated value in (19). The number of cycles N^{MES} is another vital battery life index. It counts the battery charge exchanged with the grid as in (20). When the battery stores a rated capacity $\mathbb{E}^{MES}$ and discharge it back, N^{MES} is incremented by $1 \times \mathbb{E}^{MES}$. The total ESS number of cycles $\overline{TN^{ES}}$ is imposed by (21), and it depends on the battery technology.

$$E^{MES}_{sc,y,t+1} = E^{MES}_{sc,y,t} + \sum_i (\eta^{ch} ch^{MES}_{sc,y,t}(i) - \eta^{dc} dc^{MES}_{sc,y,t}(i))\tau \tag{18}$$

$$0 \le E^{MES}_{sc,y,t} \le \mathbb{E}^{MES} \tag{19}$$

$$N^{MES}_{sc,y,t} = N^{MES}_{sc,y,t-1} + \frac{\sum_i (\eta^{ch} ch^{MES}_{sc,y,t}(i) - \eta^{dc} dc^{MES}_{sc,y,t}(i))\tau}{2} \tag{20}$$

$$\sum_{sc} \rho_{sc} \sum_y \sum_t N^{MES}_{sc,y,t=24} \le \overline{TN}\,\mathbb{E}^{MES} \tag{21}$$

C. POWER FLOW MODEL

A radial distribution feeder has a single slack bus at the substation (indexed $i = 0$), and the other buses are PQ-buses (indexed $i \epsilon \mathcal{N}^{bus}, i \neq 0$). The buses connect a group of branches l: $(i \to j) \in \psi$. In the power flow model, the change in bus active and reactive power $\Delta p^{bus}_{sc,y,t}(i)$, $\Delta q^{bus}_{sc,y,t}(i)$ leads to a change in each node voltage amplitude and angle. For a set of buses $\mathcal{N}^{bus}$, the bus power is the sum of RESs, loads, and DG units powers at this bus (22)-(24). The injected power has a negative sign whereas the absorbed power has positive value; thus, the MESS discharge power has a negative value. The loads are modeled as constant power loads with a power factor pf, thus the load reactive power is a constant ratio of the active power as $q^{Load}_{sc,y,t} = \lambda^{load}_{sc,y,t} p^{Load}_{sc,y,t}, \lambda^{load}_{sc,y,t} = \tan(\cos^{-1} pf)$. The RES reactive power is modeled by tuning $q^{res}_{sc,y,t}$, and in such a case, an apparent power constraint for RES is simply added. Further, load shedding and power curtailment can be added, if desired, as negative decision variables.

$$p^{bus}_{sc,y,t}(i) = p^{Load}_{sc,y,t}(i) - p^{res}_{sc,y,t}(i) - p^{DG}_{sc,y,t}(i) + p^{MES}_{sc,y,t}(i) \tag{22}$$

$$q^{bus}_{sc,y,t}(i) = (\lambda^{load}_{sc,y,t} p^{Load}_{sc,y,t}(i) - q^{DG}_{sc,y,t}(i) + q^{MES}_{sc,y,t}(i) \tag{23}$$

$$\Delta p^{bus}_{sc,y,t}(i) = p^{MES}_{sc,y,t}(i) \tag{24}$$

$$\Delta q^{bus}_{sc,y,t}(i) = -q^{res}_{sc,y,t}(i) \tag{25}$$

Many publications discussed the power flow relaxation and convexication in the literature [34], [35]. The second-order cone programming is one of the power flow approximations [11], [36]. Another simple linear technique depends on calculating the voltage Jacobian from the power flow (voltage sensitivity to active and reactive power) [37]. The advantage of the sensitivity technique is the resulting linear equality constraints that simplify the optimization problem. The power losses sensitivity is similarly calculated as in [38], [39]. The total power loss is linearized as the sum of the initial power losses, and the losses change due to the MESS buses power change as in (26)-(27). Finally, the slack bus power equals all buses power plus the total power losses [15] as shown in (28)-(29).

$$p^{loss}_{sc,y,t} = ip^{loss}_{sc,y,t} + \left.\frac{dp^{loss}}{dP^{bus}}\right|_{sc,y,t} \Delta P^{bus}_{sc,y,t} + \left.\frac{dp^{loss}}{dQ^{bus}}\right|_{sc,y,t} \times \Delta Q^{bus}_{sc,y,t} \tag{26}$$

$$q^{loss}_{sc,y,t} = iq^{loss}_{sc,y,t} + \left.\frac{dq^{loss}}{dP^{bus}}\right|_{sc,y,t} \Delta P^{bus}_{sc,y,t} + \left.\frac{dq^{loss}}{dQ^{bus}}\right|_{sc,y,t} \times \Delta Q^{bus}_{sc,y,t} \tag{27}$$

$$p^{grid}_{sc,y,t} = p^{bus}_{sc,y,t}(i=0) = \sum_{i,i\neq 0} p^{bus}_{sc,y,t}(i) + p^{loss}_{sc,y,t} \tag{28}$$

$$q^{grid}_{sc,y,t} = q^{bus}_{sc,y,t}(i=0) = \sum_{i,i\neq 0} q^{bus}_{sc,y,t}(i) + q^{loss}_{sc,y,t} \tag{29}$$

It is worth mentioning that the optimization problem aims indirectly at reducing the energy losses cost because it subtracts the income from the grid energy cost. $(inc - c^{grid} = \sum_{sc,y,t} \rho_{sc} \left(sp_{sc,y,t} - bp_{sc,y,t}\right) \sum_i p^{Load}_{sc,y,t}(i)\,\tau - bp_{sc,y,t} p^{loss}_{sc,y,t})$.

Branches' power values are calculated by the power balance expression in (30)-(31), which indicates that the branch power equals the branch output bus power plus the power transferred to other branches connected to it [36]. The branch

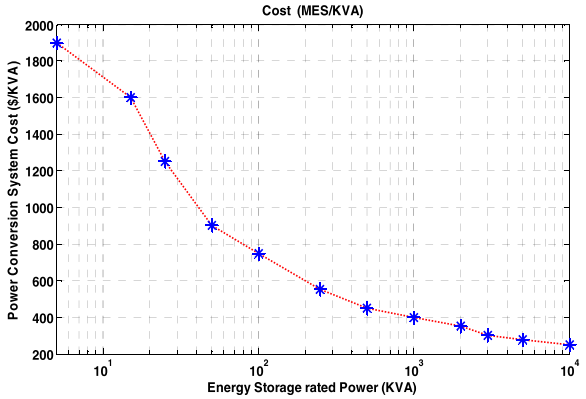

FIGURE 2. Power conversion system cost versus rated power.

ampacity is limited by (33), where the feeder apparent power $s^{f}_{sc,y,t}(l)$ is limited by the nominal feeder thermal capacity $\mathbb{S}^{f}(l)$.

$$p^{f}_{sc,y,t}(l) = p^{bus}_{sc,y,t}(j) + \sum_{k:(j\to n)\in\psi} p^{f}_{sc,y,t}(k), l:(i\to j) \tag{30}$$

$$q^{f}_{sc,y,t}(l) = q^{bus}_{sc,y,t}(j) + \sum_{k:(j\to n)\in\psi} q^{f}_{sc,y,t}(k), l:(i\to j) \tag{31}$$

$$s^{f2}_{sc,y,t} = p^{f2}_{sc,y,t} + q^{f2}_{sc,y,t} \tag{32}$$

$$\left\| s^{f}_{sc,y,t}(l) \right\| \le \mathbb{S}^{f}(l) \tag{33}$$

Regarding the voltage level, the initial voltage $iv_{sc,y,t}$ and voltage sensitivity $\frac{dv(i)}{dP^{bus}}\Big|_{sc,y,t}$, $\frac{dv(i)}{dQ^{bus}}\Big|_{sc,y,t}$ are calculated by solving the power flow using the Newton-Raphson iterative technique. This information is used in (34) to find the bus voltage. Finally, the voltage levels are constrained in (35) for power quality measurements (voltage drop and rise limits).

$$v_{sc,y,t}(i) = iv_{sc,y,t} + \frac{dv(i)}{dP^{bus}}\Big|_{sc,y,t} \Delta P^{bus}_{sc,y,t} + \frac{dv(i)}{dQ^{bus}}\Big|_{sc,y,t} \times \Delta Q^{bus}_{sc,y,t} \tag{34}$$

$$\underline{v} \le v_{sc,y,t}(i) \le \overline{v} \tag{35}$$

After including all the previous constraints, the resulting sizing problem (36) is a mixed-integer nonlinear problem due to the MESS constraints (14)-(17). Further, the cost function is a nonlinear function of the storage rated-power-dependent cost as shown in Figure 2. The decision variables of this problem include the MESS rated power and capacity $\mathbb{S}^{MES}$, $\mathbb{E}^{MES}$, and the MESS stations set $\mathbb{z}^{MES}$. Other variables that result from the optimization process represent the system operation nature during different scenarios, years and samples. These variables help the operator to study the system performance under the planning decision results. These variables include the instantaneous MESS location set $\mathbb{x}^{MES} = \bigcup_{Sc,y,t,i} x^{MES}_{sc,y,t}(i)$ and similarly, the active, reactive power, and voltage sets: $\mathbb{P}^{MES} = \bigcup_{Sc,y,t,i} p^{MES}_{sc,y,t}(i), \mathbb{Q}^{MES} = \bigcup_{Sc,y,t,i} q^{MES}_{sc,y,t}(i) \mathbb{v}^{MES} = \bigcup_{Sc,y,t,i} v^{MES}_{sc,y,t}(i)$, and similarly the battery dynamics, such as the capacity and number of cycles.

$$\max_{\mathbb{S}^{MES},\mathbb{E}^{MES},\mathbb{z}^{MES},\mathbb{x}^{MES},\mathbb{P},\mathbb{Q},\mathbb{v}} (pro)$$
$$s.t. \begin{cases} MESS\ dynamical\ model: (5)-(19) \\ Power\ flow\ model: (20)-(33) \end{cases} \tag{36}$$

III. PROPOSED ALGORITHM

The sizing optimization problem (36) is a mixed-integer nonconvex problem (nondeterministic polynomial time) that may face feasibility problems. This section proposes a two-stages optimization technique to make (36) solutions less complex.

- First, the particle swarm optimization is utilized to detect the optimal MESS rated power ($\mathbb{S}^{ES}$) and stations optimal locations ($\mathbb{z}^{MES}$).
- By substituting ($\mathbb{S}^{ES}$) and ($\mathbb{z}^{MES}$) values in (36), the problem becomes a mixed-integer convex problem. The problem can be easily solved to find the optimum MESS capacity.

This technique utilizes both the heuristic and gradient-based optimization methods.

The PSO is a smart iterative search method that changes the decision variables (swarm positions) to optimize a certain criterion [40]. In this paper, the PSO changes the MESS rated power and locations such that the profit is maximized. The proposed algorithm is described in the following steps.

1- The PSO generates a random initial population of particles $\mathbb{Y}(j=0)$, which is defined by M particles size as in (37). Each particle at certain iteration j, $y(j)$ consists of the MESS rated power $\mathbb{S}^{MES}_{m}(j)$ with its associated cost and a proposed locations set $\mathbb{z}^{MES}_{m}(j)$ as in (38).

$$\mathbb{Y}(j) = [y_1(j), y_2(j), \ldots, y_m(j), \ldots y_M(j)] \tag{37}$$

$$y_m(j) = [\mathbb{S}^{MES}_{m}(j), \mathbb{z}^{MES}_{m}(j)] \to c_m{}^{MES/MVA}(j) \tag{38}$$

2- The following constraints in (39)-(40) are imposed on all particles to keep the rated power within the allowable range and define the locations' binary sets.

$$0 \le \mathbb{S}^{MES}_{m}(j) \le \overline{\mathbb{S}^{MES}} \tag{39}$$

$$\mathbb{z}^{MES}_{m}(j) \in \{0, 1\} \tag{40}$$

3- For each particle, the associated profit is calculated by solving the mixed-integer convex problem (41). The problem is as in (36) after the following modifications:
a) The MESS location set becomes a parameter decided by each particle.
b) The nonlinear constraints (14)-(17) become convex (linear or quadratic) after considering the MESS rated power a constant parameter.
c) The rated power cost is calculated from an interpolation table follows Figure 2. Now, this problem is efficiently solved by solvers such as GUROBI [41].

4- The resulting capacity is also saved for each solution after solving (41) as expressed in (42)

$$\max_{\mathbb{E}^{MES},\mathbb{x}^{MES},\mathbb{P},\mathbb{Q},\mathbb{v}} \left(pro_m(j) = pro(y_m(j), c_m^{MES/MVA}(j))\right)$$

$$s.t. \begin{cases} MESS\ dynamical\ model: (5)-(7), (10), (11), (16)-(19) \\ Power\ flow\ model: (22)-(33) \\ \mathbb{Z}^{MES} = \mathbb{z}_m^{MES}(j) \\ 0 \le ch_{sc,y,t}^{MES}(i) \le \mathbb{S}_m^{MES}(j) x_{sc,y,t}^{MES}(i) \\ -\mathbb{S}_m^{MES}(j) x_{sc,y,t}^{MES}(i) \le dc_{sc,y,t}^{MES}(i) \le 0 \\ -\mathbb{S}_m^{MES}(j) x_{sc,y,t}^{MES}(i) \le q_{sc,y,t}^{MES}(i) \le \mathbb{S}_m^{MES}(j) x_{sc,y,t}^{MES}(i) \\ p_{sc,y,t}^{MES}(i)^2 + q_{sc,y,t}^{MES}(i)^2 \le x_{sc,y,t}^{MES}(i)\, \mathbb{S}_m^{MES}(j)^2 \end{cases} \quad (41)$$

$$\mathbb{E}_m^{MES}(j) = \left\{ \mathbb{E}^{MES} \,|\, \arg\{\max_{\mathbb{E},\mathbb{x}} (pro_m(j))\} \right\} \quad (42)$$

At each iteration J, the local and global best positions are updated as follows:

$$y^{loc}(j=J) = \left\{ y_\beta(J) \,|\, pro_\beta(J) > pro_m(J) \forall m \right\} \quad (43)$$

$$y^{Glo}(J) = \left\{ y_\alpha \,|\, pro_\alpha > pro_m(j)\ \forall m, \forall j \le J \right\} \quad (44)$$

5- Depending on the iteration J, the new inertia ω and speed vectors V are found from (45)-(46), the speed is inclined to both the local and global best positions depending on the factors c_1, c_2. Finally, the speed is used to update all particles positions as shown in (48) after checking its limits in (47).

$$\omega(j) = \omega_{max} - \frac{\omega_{max} - \omega_{min}}{\bar{J}} j \quad (45)$$

$$V_m(j+1) = \omega(j) V_m(j) + c_1 r_1 (y^{loc}(j) - y_m(j)) + c_2 r_2 (y^{Glo}(j) - y_m(j)) \quad (46)$$

$$-\overline{V}_m \le V_m(j+1) \le \overline{V}_m \quad (47)$$

$$y_m(j+1) = V_m(j+1) + y_m(j) \quad (48)$$

Step 2 is repeated as long as the stopping criterion is not triggered. There are two stopping criteria. First, if the maximum number of iterations $\bar{j}$ is reached. Second, if the profit percentage change stayed within a pre-calculated tolerance zone ε for a certain number of iterations γ as given in (50).

$$j \ge \bar{j} \quad (49)$$

$$\Delta pro^{Glo}(j : j+\gamma) \le \varepsilon, \quad j+\gamma \le \bar{j} \quad (50)$$

6- Finally, if the stopping criterion is achieved, an optimum sizing and allocation decision is reached. Figure 3 shows the flowchart of the proposed optimization framework.

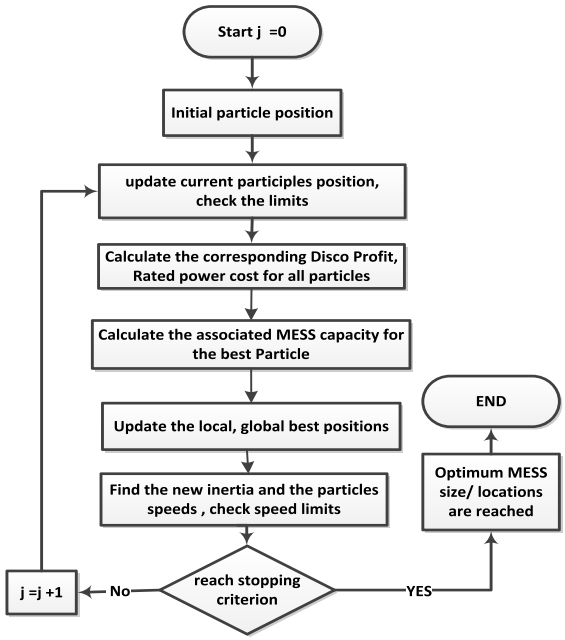

FIGURE 3. Hybrid optimization scheme for MESS sizing and allocation.

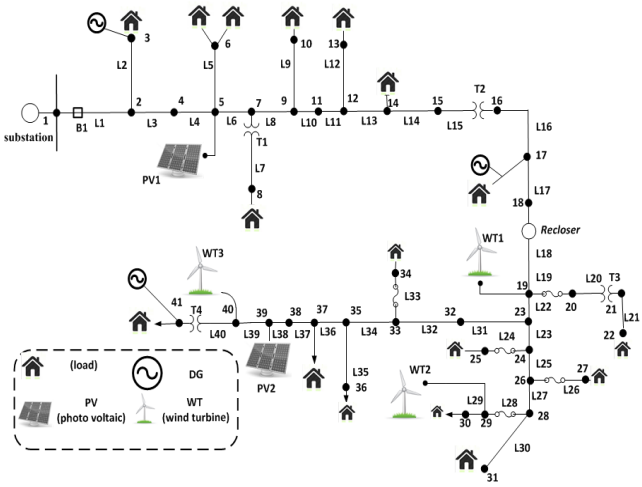

FIGURE 4. Single-line diagram for the distribution feeder under study.

IV. CASE STUDY

The MESS sizing algorithm is validated by simulating it on a real radial feeder in Ontario-Canada. The 30 km feeder is connected to the transmission system via a 16 MVA substation [42] as shown in Figure 4. The feeder consists of 41-buses with three DG units that operate daily during peak-hours (5:8 pm). The rated power of DG units and RESs is given in Table 1. The feeder parameters are given in [42]. A daily realistic residential load profile is adopted (provided in [43]) and depicted in Figure 5(a). Two PV plants (PV1, PV2) have a generation profile used from [44], as shown in Figure 5(b), whereas three wind facilities (WT1, WT2, WT3) are dispersed on the feeder. A real market energy price is taken from [45]. Typical wind profiles in [46] are used and shown in Figure 5(d). The total RES penetration of this feeder

TABLE 1. Optimization input parameters.

RES , DG units rating	$p^{wt1} = 2MW, p^{wt2} = p^{wt3} = 1.5MW, p^{DG_1} = 1\ MW$ $p^{pv_1} = p^{pv_2} = 0.5\ MW\ , p^{DG_2} = p^{DG_3} = 0.5\ MW$ $\mathcal{N}^{MES}\ candidates = \{4, 6, 9, 12, 22, 25, 28, 35, 39, 40\}$
MESS data	$\underline{v} = 0.95, \bar{v} = 1.05, \tau = 1, IR = 3\%, Y = 12, Sc = 48,$ $\overline{\mathbb{S}^{MES}} = 5\ MVA, \overline{\mathbb{E}^{ES}} = 15MWh, FC^{MES} = 5000\$,$ $C^{truck} = 50K\$, \overline{DT} = 4, \alpha^{TN} = 20\%$ $\overline{DN^{MES}} = 1, \overline{TN^{MES}} = 3000, \overline{z^{MES}} = 3, O\&M^{MES} = 42k\$/y$ $C^{MES/_{MWh}} = 600\ K\$, \eta = 0.85$
PSO data	$\bar{J} = 200, c_1 = c_2 = 2, \omega_{max} = 0.9, \omega_{min} = 0.1$ $M = 10, \gamma = 8, \varepsilon = 0.25\%, \overline{V_m} = [0.5 * ones(10,1); 1\ ]$

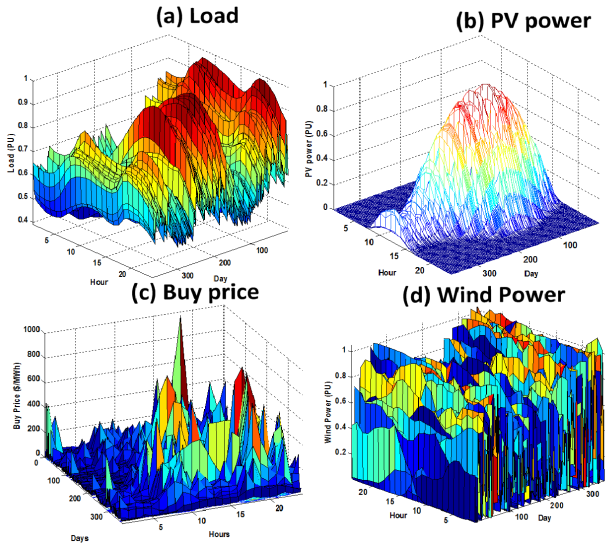

FIGURE 5. The first-year input data (a) Daily load profile in P.U (b) PV generated power in P.U (c) Market price given in $/MWh and (d) Generated wind power in P.U.

reaches 37%. The energy sell price is assumed to a fixed monthly tariff as adopted by the distribution utility company (e.g., [47], [48]). To account for the MESS transition delay, the MESS truck average speed is assumed 60 km/hour, the distance between buses is given in [30]. The transition delay is calculated accordingly.

Twelve years of historical market and power data are used in the sizing problem as real scenarios (realizations) to cover the whole planning horizon. The twelve years scenarios will lead to an enormous problem size; thus, similar to [11], a realizations reduction using the k-means technique is adopted. Using an hourly sample rate, each daily realization consists of (PV, load, wind and price data) vector with a dimension 1×96. To reduce the number of daily realizations (here $365 \times 12 = 4380$) to SC scenarios, the k-means clustering method approximates each year's realizations by four centroids (scenarios) to mimic each season. The resulting total scenarios $SC = 4 \times 12 = 48$, each is a vector with dimension 1×96. The Euclidian distance of each realization to a certain centroid defines the realization belonging to it, and by so, the scenario probability is calculated as a function of the sum of these distances.

TABLE 2. Optimization results with different ESS technologies.

	MESS
Rated power	3250 KVA
Capacity	6381.3 KWh
Optimal locations	9 (St.1), 28 (St.2), 40 (St.3)
Power converter cost	418,220$
Battery bank costs	3,828,780$
MESS capital cost	4,247,000 $
Transition delay cost	109,500$
Losses reduction	47.22%
Max. Load reduction	4.38%
Saved losses	2,092,500 $
Arbitrage profit	2,919,800 $
Total profit	10,138,000$
Profit increase	295,900 $

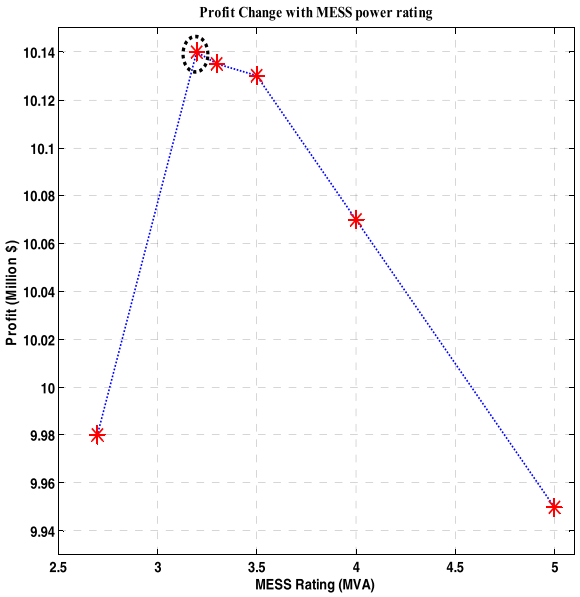

FIGURE 6. MESS rated power verses Profit.

Regarding the MESS, the lithium-ion battery is adopted due to its high energy intensity, high efficiency, and long life. The battery technical and economic data are taken from [49]. The storage life cycles are 3000 life cycles during the planning period. The power conversion cost follows Figure 2, whereas the yearly operation and maintenance cost is assumed 12 k$/year (assuming a part-time driver with two hours duty daily), and the truck capital cost is assumed 50 k$. For the MESS stations allocation, ten buses are chosen as candidates as given in Table 1; only three buses are allowed as MESS stations. The PSO parameters are set using trial and error, and the population size was found to provide adequate computational time for this particular problem. For defining the MESS daily number of trips $\overline{DT}$, the minimum value is desirable given that it achieves the maximum profit and guarantees a feasible solution. Here, $\overline{DT}$ was found to be four.

Table 2 shows the economic results of the MESS during the whole operation period including different costs and income to the Disco. From Figure 2, the MESS power converter cost

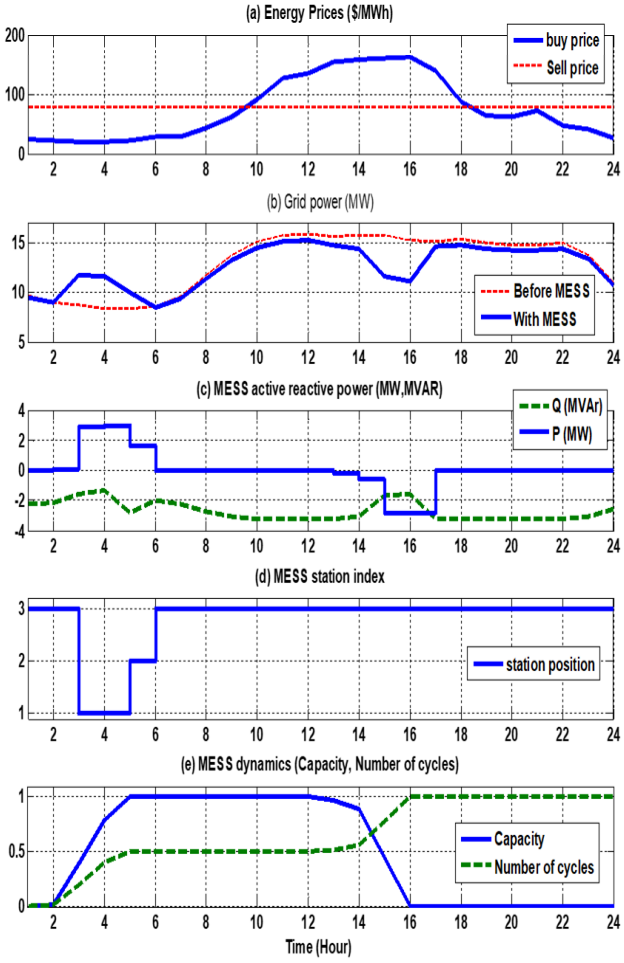

FIGURE 7. Summer day scenario results (a) Energy buy and sell prices (b) grid-purchased power (after/before) MESS (c) MESS active and reactive Powers (d) MESS location (station). (e) Capacity and number of cycles.

has approximately 200 k$ in savings as compared to buying three distributed ESSs converters. Further, the MESS has managed to gain a significant arbitrage profit, and achieve a higher losses saving due to improving the voltage profile.

Furthermore, a significant maximum load reduction is reached, which will defer substation or feeder upgrade cost for the Disco. Overall, the MESS is proved to be a profitable investment to the Disco under the given prediction scenarios.

Regarding the MESS stations allocations, three locations are chosen as an optimum solution; one near the feeder substation {bus 9}, and the other two at each lateral's end {buses 28, 40}. A good explanation for this result is that the MESS is supposed to provide voltage regulation at the weakest far-away buses.

Regarding the optimality of the resulting MESS sizing, Figure 6 compares the profit with different MESS power ratings. It is concluded that the proposed algorithm has managed to define an optimum solution.

To monitor the dynamic performance of the MESS, winter day scenarios are shown in Figure 7. During this scenario, the MESS shifts the late-night energy to the afternoon peak hour to achieve arbitrage profit, as shown in Figure 7(b). Regarding the MESS location transitions, first, the MESS provides leading reactive power support at the feeder far end (Station 3 (St. 3) or bus 40), then it moves to bus 9 to start charging. The reason for this transition is reducing the power losses by choosing a charging location near the main substation. The second transition is made to bus 28 (St. 2), near WT3 where the extra wind power is saved for the peak hour. After charging the surplus wind energy, the MESS moves to the feeder end (at St. 3 located at bus 40), where the MESS performs voltage regulation with energy arbitrage (discharging the stored off-peak energy during the peak hour).

Regarding the number of the MESS trips, it is kept under four as given in the optimization constraints and depicted in Figure 7(d). Besides, the capacity is upper-bounded by the rated value, and the number of charging cycles is one as shown in Figure 7(e). No overcharge or excessive charging cycles have occurred thanks to constraints (18), (20).

It is worth mentioning that the MESS positioning strategy will change if it does not participate in voltage regulation (omit constraint (48), and instead add static VAr compensators or capacitors). This is all up to the Disco that may prefer different energy management strategies for the MESS.

V. CONCLUSION

This paper proposed a sizing and allocation algorithm for a MESS in a power distribution system. The sizing problem aims at maximizing the distribution company profit by considering the participation of the MESS in multi grid-support services including energy arbitrage, voltage regulation, and power losses minimization. The sizing constraints include the battery life cycles and dynamic capacity, and take into account the feeder voltage levels and ampacity. Load and renewable energy variations are modeled via considering different scenarios in the sizing scheme. Further, a size-dependent cost for the power converter is adopted for more realistic and practical results. The sizing algorithm is tested by a simulation case study on a real feeder in Ontario, Canada. The study results have shown that using the MESS can maintain the system power quality constraints while achieving profit for the distributed system operator.

REFERENCES

[1] M. Arif, A. Oo, and A. Ali, "Energy storage: Applications and advantages," in *Smart Grids: Opportunities, Developments, and Trends*. New York, NY, USA: Springer, 2013, pp. 77–109.

[2] S. Vazquez, S. M. Lukic, E. Galvan, L. G. Franquelo, and J. M. Carrasco, "Energy storage systems for transport and grid applications," *IEEE Trans. Ind. Electron.*, vol. 57, no. 12, pp. 3881–3895, Dec. 2010.

[3] F. Garcia-Torres and C. Bordons, "Optimal economical schedule of hydrogen-based microgrids with hybrid storage using model predictive control," *IEEE Trans. Ind. Electron.*, vol. 62, no. 8, pp. 5195–5207, Aug. 2015.

[4] S. T. Kim, S. Bae, Y. C. Kang, and J. W. Park, "Energy management based on the photovoltaic HPCS with an energy storage device," *IEEE Trans. Ind. Electron.*, vol. 62, no. 7, pp. 4608–4617, Jul. 2015.

[5] H. Beltran, E. Bilbao, E. Belenguer, I. Etxeberria-Otadui, and P. Rodriguez, "Evaluation of storage energy requirements for constant production in PV power plants," *IEEE Trans. Ind. Electron.*, vol. 60, no. 3, pp. 1225–1234, Mar. 2013.

[6] P. Li, R. Dargaville, F. Liu, J. Xia, and Y.-D. Song, "Data-based statistical property analyzing and storage sizing for hybrid renewable energy systems," *IEEE Trans. Ind. Electron.*, vol. 62, no. 11, pp. 6996–7008, Nov. 2015.

[7] D. Rastler, A. Akhil, D. Gauntlett, and E. Cutter, *Energy Storage System Costs 2011 Update Executive Summary*. Palo Alto, CA, USA: EPRI, 2012.

[8] H. H. Abdeltawab and Y. A.-R. I. Mohamed, "Mobile energy storage scheduling and operation in active distribution systems," *IEEE Trans. Ind. Electron.*, vol. 64, no. 9, pp. 6828–6840, Sep. 2017.

[9] P. Fortenbacher, A. Ulbig, and G. Andersson, "Optimal placement and sizing of distributed battery storage in low voltage grids using receding horizon control strategies," *IEEE Trans. Power Syst.*, vol. 33, no. 3, pp. 2383–2394, May 2018.

[10] M. S. Taha, H. H. Abdeltawab, and Y. A.-R. I. Mohamed, "An online energy management system for a grid-connected hybrid energy source," *IEEE J. Emerg. Sel. Topics Power Electron.*, vol. 6, no. 4, pp. 2015–2030, Dec. 2018.

[11] M. Nick, R. Cherkaoui, and M. Paolone, "Optimal allocation of dispersed energy storage systems in active distribution networks for energy balance and grid support," *IEEE Trans. Power Syst.*, vol. 29, no. 5, pp. 2300–2310, Sep. 2014.

[12] I. N. Moghaddam, B. H. Chowdhury, and S. Mohajeryami, "Predictive operation and optimal sizing of battery energy storage with high wind energy penetration," *IEEE Trans. Ind. Electron.*, vol. 65, no. 8, pp. 6686–6695, Aug. 2018.

[13] Y. Yang, Q. Ye, L. J. Tung, M. Greenleaf, and H. Li, "Integrated size and energy management design of battery storage to enhance grid integration of large-scale PV power plants," *IEEE Trans. Ind. Electron.*, vol. 65, no. 1, pp. 394–402, Jan. 2018.

[14] Y. Dvorkin, R. Fernández-Blanco, Y. Wang, B. Xu, D. S. Kirschen, H. Pandžic, J.-P. Watson, and C. A. Silva-Monroy, "Co-planning of investments in transmission and merchant energy storage," *IEEE Trans. Power Syst.*, vol. 33, no. 1, pp. 245–256, Jan. 2018.

[15] S. Chakraborty, T. Senjyu, H. Toyama, A. Y. Saber, and T. Funabashi, "Determination methodology for optimising the energy storage size for power system," *IET Generat., Transmiss. Distrib.*, vol. 3, no. 11, pp. 987–999, Nov. 2009.

[16] H. Pandžić, Y. Wang, T. Qiu, Y. Dvorkin, and D. S. Kirschen, "Near-optimal method for siting and sizing of distributed storage in a transmission network," *IEEE Trans. Power Syst.*, vol. 30, no. 5, pp. 2288–2300, Sep. 2014.

[17] S. Wogrin and D. F. Gayme, "Optimizing storage siting, sizing, and technology portfolios in transmission-constrained networks," *IEEE Trans. Power Syst.*, vol. 30, no. 6, pp. 3304–3313, Nov. 2015.

[18] I. Alsaidan, A. Khodaei, and W. Gao, "A comprehensive battery energy storage optimal sizing model for microgrid applications," *IEEE Trans. Power Syst.*, vol. 33, no. 4, pp. 3968–3980, Jul. 2018.

[19] H. Xie, X. Teng, Y. Xu, and Y. Wang, "Optimal energy storage sizing for networked microgrids considering reliability and resilience," *IEEE Access*, vol. 7, pp. 86336–86348, 2019.

[20] S. X. Chen, H. B. Gooi, and M. Q. Wang, "Sizing of energy storage for microgrids," *IEEE Trans. Smart Grid*, vol. 3, no. 1, pp. 142–151, Mar. 2012.

[21] C. Abbey and G. Joos, "A stochastic optimization approach to rating of energy storage systems in wind-diesel isolated grids," *IEEE Trans. Power Syst.*, vol. 24, no. 1, pp. 418–426, Feb. 2009.

[22] Y. Zheng, Z. Dong, S. Huang, K. Meng, F. Luo, J. Huang, and D. Hill, "Optimal integration of mobile battery energy storage in distribution system with renewables," *J. Mod. Power Syst. Clean Energy*, vol. 3, no. 4, pp. 589–596, 2015.

[23] Y. Chen, Y. Zheng, F. Luo, J. Wen, and Z. Xu, "Reliability evaluation of distribution systems with mobile energy storage systems," *IET Renew. Power Gener.*, vol. 10, no. 10, pp. 1562–1569, 2016.

[24] D. Rastler, *Transportable Energy Storage Systems Project*. Palo Alto, CA, USA: EPRI, 2009.

[25] D. Rastler, *Technical Specification for a Transportable Lithium-Ion Energy Storage System for Grid Support Using Commercially Available Lithium-Ion Technology*. Palo Alto, CA, USA: EPRI, 2012.

[26] N. Nakhodchi, N. Aghli, S. Alishahi, and M. H. Pourarab, "Design and successful utilisation of the first multi-purpose mobile distributed energy storage system in Iran," *CIRED-Open Access Proc. J.*, vol. 2017, no. 1, pp. 109–111, 2017.

[27] DOE. *Fujian Electric Power Research Institute Mobile Energy Storage Station I*. Department of Energy, New York, NY, USA. Accessed: Jul. 30, 2015. [Online]. Available: http://www.energystorageexchange.org/projects/153

[28] Winston-Battery. (2015). *Mobile Power Storage*. Winston Energy Group Limited. Accessed: Jul. 30, 2015. [Online]. Available: http://en.winston-battery.com/index.php/products/mobile-power

[29] Toshiba. (2014). *Spain's Gas Natural Fenosa and Toshiba to Demonstrate Use of Transportable Lithium-ion Battery Energy Storage System in Power Distribution Network*. Accessed: Jul. 30, 2015. [Online]. Available: https://www.toshiba.co.jp/about/press/2014_01/pr0704.htm

[30] H. M. Abdeltawab, *Planning and Energy Management of Energy Storage Systems in Active Distribution Networks*. Edmonton, AB, Canada: Univ. of Alberta, 2017.

[31] A. Yazdani and R. Iravani, *Voltage-Sourced Converters in Power Systems*. Hoboken, NJ, USA: Wiley, 2010.

[32] H. H. Abdeltawab and Y. A.-R. I. Mohamed, "Market-oriented energy management of a hybrid wind-battery energy storage system via model predictive control with constraint optimizer," *IEEE Trans. Ind. Electron.*, vol. 62, no. 11, pp. 6658–6670, Nov. 2015.

[33] A. S. A. Awad, T. H. M. EL-Fouly, and M. M. A. Salama, "Optimal ESS allocation for load management application," *IEEE Trans. Power Syst.*, vol. 30, no. 1, pp. 327–336, Jan. 2015.

[34] L. Gan, N. Li, S. H. Low, and U. Topcu, "Exact convex relaxation of optimal power flow in radial networks," *IEEE Trans. Autom. Control*, vol. 60, no. 1, pp. 72–87, Jan. 2015.

[35] J. Lavaei, D. Tse, and B. Zhang, "Geometry of power flows and optimization in distribution networks," *IEEE Trans. Power Syst.*, vol. 29, no. 2, pp. 572–583, Mar. 2014.

[36] W. Shi, X. Xie, C. C. Chu, and R. Gadh, "Distributed optimal energy management in microgrids," *IEEE Trans. Smart Grid*, vol. 6, no. 3, pp. 1137–1146, May 2015.

[37] K. Christakou, J.-Y. LeBoudec, M. Paolone, and D.-C. Tomozei, "Efficient computation of sensitivity coefficients of node voltages and line currents in unbalanced radial electrical distribution networks," *IEEE Trans. Smart Grid*, vol. 4, no. 2, pp. 741–750, Jun. 2013.

[38] M. Hong, "An approximate method for loss sensitivity calculation in unbalanced distribution systems," *IEEE Trans. Power Syst.*, vol. 29, no. 3, pp. 1435–1436, May 2014.

[39] S.-J. Lee and S.-D. Yang, "Derivation of P-Q loss sensitivities by angle reference transposition and an application to optimal P-Q generation for minimum cost," *IEEE Trans. Power Syst.*, vol. 21, no. 1, pp. 428–430, Feb. 2006.

[40] J. Kennedy and R. Eberhart, "Particle swarm optimization," in *Proc. Int. Conf. Neural Netw. (ICNN)*, Perth, WA, Australia, Dec. 1995, pp. 1942–1948.

[41] Gurobi. *Gurobi Optimization*. Accessed: Aug. 18, 2015. [Online]. Available: http://www.gurobi.com/

[42] Y. Atwa, *Distribution System Planning and Reliability Assessment under High DG Penetration*. Waterloo, ON, Canada: Univ. of Waterloo, 2010.

[43] PJM. (2015). *Meterd Load Data*. Accessed: Dec. 1, 2015. [Online]. Available: http://www.pjm.com/markets-and-operations/ops-analysis/historical-load-data.aspx

[44] SODA. (2015). *Solar Energy Services for Professionals*. Accessed: Dec. 1, 2015. [Online]. Available: http://www.soda-is.com/eng/index.html

[45] AESO. *Market & System Reporting*. Accessed: Apr. 4, 2016. [Online]. Available: http://www.aeso.ca/market/8856.html

[46] AESO. (2015). *Alberta Electric System Operator*. [Online]. Available: http://www.aeso.ca/gridoperations/20544.html

[47] AESO. (2015). *Alberta Electric System Operator*. [Online]. Available: http://www.aeso.ca/market/23873.html

[48] EPCOR. (2015). *Residential Rates & Fees*. [Online]. Available: http://www.epcor.com/power-natural-gas/regulated-rate-option/Pages/residential-rates.aspx

[49] S. Schoenung, *Energy Storage Systems Cost Update; A Study for the DOE Energy Storage Systems Program*. Albuquerque, NM, USA: Sandia National Laboratories, Apr. 2011.

HUSSEIN ABDELTAWAB (GS'12–M'17) was born in Bani-Souwaif, Egypt, in April 1987. He received the B.Sc. (Hons.) and M.Sc. degrees in electrical engineering from Cairo University, in 2009 and 2012, respectively, and the Ph.D. degree in electrical engineering from the University of Alberta, Edmonton, AB, Canada, in 2017. He is currently an Assistant Teaching Professor of electrical engineering with Penn State University, Altoona, PA, USA. He is also a licensed Professional Engineer in Alberta, Canada. His research interests include energy management, control system applications in renewable energy, energy storage, and smart distribution systems.

YASSER ABDEL-RADY I. MOHAMED (M'06–SM'11) was born in Cairo, Egypt, in November 1977. He received the B.Sc. (Hons.) and M.Sc. degrees in electrical engineering from Ain Shams University, Cairo, in 2000 and 2004, respectively, and the Ph.D. degree in electrical engineering from the University of Waterloo, Waterloo, ON, Canada, in 2008. He is currently a Professor with the Department of Electrical and Computer Engineering, University of Alberta, AB, Canada. His research interests include dynamics and controls of power converters, grid integration of distributed generation and renewable resources, microgrids, modeling, analysis, and control of smart grids, and electric machines and motor drives. He is also a registered Professional Engineer in the Province of Alberta. He is an Associate Editor of the IEEE TRANSACTIONS ON POWER ELECTRONICS and an Editor of the IEEE TRANSACTIONS ON POWER SYSTEMS, the IEEE TRANSACTIONS ON SMART GRID, and the IEEE POWER ENGINEERING LETTERS.